Weaver, P.P.E., Schmincke, H.-U., Firth, J.V., and Duffield, W. (Eds.), 1998
Proceedings of the Ocean Drilling Program, Scientific Results, Vol. 157

24. PRE-ERUPTIVE H_2O AND CO_2 CONTENTS OF MAFIC MAGMAS FROM THE SUBMARINE TO EMERGENT SHIELD STAGES OF GRAN CANARIA[1]

Paul J. Wallace[2]

ABSTRACT

Volcaniclastic sediments recovered from the clastic apron of Gran Canaria during Leg 157 provide a rare opportunity to study basaltic volcanism from the early shield-building phase of an oceanic island. Infrared spectroscopic analyses of trapped melt (glass) inclusions from Miocene hyaloclastites, many of which are picritic, generally show very low pre-eruptive dissolved H_2O concentrations (0.08 to ~0.2 wt% H_2O). Two glass inclusions from a differentiated basaltic hyaloclastite have significantly higher water concentrations (1.2–1.4 wt%). The speciation of water in these two inclusions is consistent with the high-temperature equilibrium for water in basaltic melts, indicating that the high total dissolved H_2O concentrations are not caused by secondary hydration. The low dissolved H_2O concentrations of most of the glass inclusions are comparable to the lowest values found in mid-ocean-ridge basalts, whereas the H_2O-rich glass inclusions are similar to the highest values reported for submarine alkalic glasses from Hawaii. Most inclusions have dissolved carbonate contents between 100 and 350 ppm CO_2. A single inclusion has a much higher CO_2 content (1426 ppm) that indicates pyroxene crystallization and inclusion entrapment at a pressure of ~2800 bars. All other inclusions must have formed by pyroxene crystallization at an average pressure of 500 ± 100 bars, equivalent to ~1–3 km depth beneath the subaerial Miocene volcanic edifice of Gran Canaria. Such low pressures of crystallization for picritic magmas suggest that during the shield-building phase of Gran Canaria, ascending batches of picritic magma were sufficiently CO_2-rich to be positively buoyant relative to shallow-stored magma. Comparison of degassing models for basaltic melts with measured vesicularities of altered glass shards from the hyaloclastites indicates that much of the glass shard and crystal debris, from which the hyaloclastites were deposited, originally formed in submarine eruptions at water depths <~500 m.

INTRODUCTION

The compositional evolution of oceanic islands has provided important insights into mantle dynamics and geochemistry. Although the subaerial stages of volcanism on many islands have been studied in detail, little is known about the geochemical evolution of the submarine stages, which typically make up more than 90% of the volume of ocean island volcanoes. Leg 157 was designed to investigate the growth of one such volcanic system, Gran Canaria, which was chosen because of its well-studied 15-m.y. subaerial history and wide spectrum of magma compositions (Schmincke, 1982; Hoernle and Schmincke, 1993; Schmincke, 1994).

Four holes drilled north (Sites 953 and 954) and south (Sites 955 and 956) of the island (Fig. 1) penetrated a total of almost 3000 m and demonstrated that the compositional evolution, growth, and mass wasting of an oceanic island is reflected in the sediments of the adjacent volcaniclastic apron (Schmincke, Weaver, Firth, et al., 1995). All major volcanic and nonvolcanic phases of Gran Canaria were recognized in the ages and compositions of sediments, physical properties, and geophysical logs. The highest rate of volcaniclastic deposition corresponds to the middle Miocene basaltic shield stage. The volcaniclastic sediments recovered from this stage consist largely of thick, graded hyaloclastite tuffs and debris flows that contain abundant altered basaltic glass shards formed by submarine eruptions (Fig. 2). These are overlain by 40 m of breccias and lapillistones that record the transition from shallow submarine to subaerial eruptions. On land, the shield basalts are covered by >200 m of felsic tuffs and lava flows (Schmincke, 1994). Different facies of volcaniclastic sediments recovered from Sites 953, 955, and 956 can be correlated with this post-shield felsic volcanic stage. After an important volcanic hiatus on Gran Canaria from 9.5 to 4.5 Ma (Schmincke, 1994), a renewed period of subaerial volcanism, which includes Pliocene to recent basaltic eruptions, once again provided clastic material to the volcanic apron.

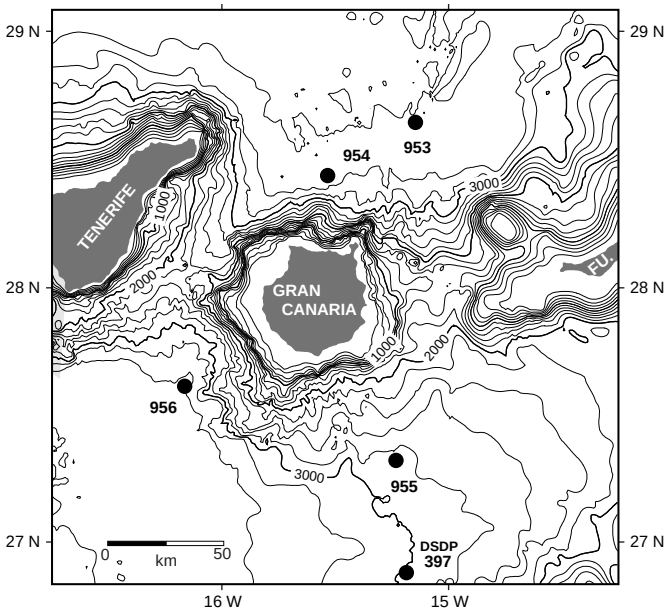

Figure 1. Map of the central Canary islands showing the locations of Leg 157 drill sites (Schmincke, Weaver, Firth, et al., 1995). Also shown for reference is the location of Deep Sea Drilling Project (DSDP) Site 397.

[1]Weaver, P.P.E., Schmincke, H.-U., Firth, J.V., and Duffield, W. (Eds.), 1998. *Proc. ODP, Sci. Results*, 157: College Station, TX (Ocean Drilling Program).

[2]Ocean Drilling Program and Dept. of Geology and Geophysics, Texas A&M University, College Station, TX 77845, U.S.A. paul_wallace@odp.tamu.edu

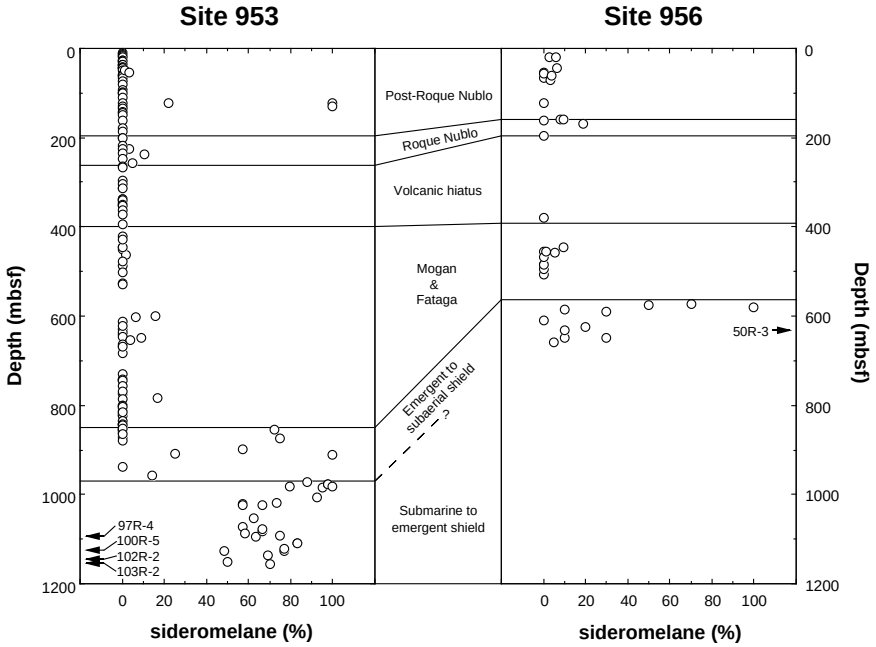

Figure 2. Modal abundance of altered basaltic glass shards (sideromelane) as a function of recovery depth (in meters below seafloor) from Sites 953 and 956. Percent sideromelane is calculated as 100 × sideromelane/(sideromelane + lithic clasts). The modal data were estimated from thin sections, as reported in Shipboard Scientific Party (1995a, 1995b); additional data for cores from the lowermost sequence at Site 956 were obtained as part of this study. The depths of core samples from which glass inclusions were analyzed (Table 1) are indicated by arrows. No inclusions large enough for IR spectroscopic analysis were found in the sediments from the emergent to subaerial shield stage at Site 953. Shown for reference are the correlations from the volcaniclastic sediments to the various subaerial volcanic phases that are well documented on Gran Canaria (e.g., Schmincke, 1994). These correlations were deduced from the petrography, mineralogy, and geochemistry of the volcaniclastic sediments from Sites 953 and 956 (Shipboard Scientific Party, 1995a, 1995b.

The goal of this study was to investigate the crystallization, degassing, and eruptive history of basaltic magmas from the Miocene submarine to emergent shield stage of Gran Canaria. I analyzed glass inclusions in clinopyroxene phenocrysts from hyaloclastites and lapillistones that correspond to this stage. Glass inclusions are samples of silicate melt that were originally trapped inside growing crystals and subsequently quenched to glass during eruption. Inclusions that remain sealed during eruption do not degas volatile elements (e.g., H_2O, CO_2, S, Cl, and F). Analysis of the included glasses can thus yield important information concerning the original dissolved volatile contents of the magmas before eruption. This is particularly important for studying the shield stage of Gran Canaria because many glass inclusions remain unaltered in submarine samples, whereas the basaltic glass shards that form a major component of the hyaloclastites and lapillistones are altered. I analyzed the inclusions for both dissolved H_2O and CO_2 to estimate the range of depths (pressures) at which the pyroxene host crystals formed. In addition, these data can be used to estimate the range of water depths at which the basaltic magmas were erupted and quenched. Most of the basaltic glass shards in the hyaloclastites from Sites 953 and 956 are slightly to moderately vesicular. Measurements of vesicle proportions in glass shards from the hyaloclastites can be combined with thermodynamic models of magma degassing to calculate the depth at which the basalts were erupted. This provides constraints on the temporal and physical evolution of the shield during the transition from submarine to subaerial eruptions.

PETROGRAPHY, GEOCHEMISTRY, AND DEPOSITIONAL HISTORY OF VOLCANICLASTIC SEDIMENTS

Site 953

The oldest volcaniclastic sediments recovered from the drill sites around Gran Canaria (Fig. 1) are middle Miocene hyaloclastite tuffs, lapillistones, and breccias from the lowermost part (969–1159 meters below seafloor [mbsf]) of Hole 953C (Shipboard Scientific Party, 1995a). The sediments contain abundant altered basaltic glass fragments (sideromelane) that vary in texture from nonvesicular to highly vesicular. Some intervals are dominated by nonvesicular to slightly vesicular shards. Olivine pseudomorphs and clinopyroxene phenocrysts are common in the sideromelane shards and as isolated crystals. The dominant lithic clasts are picritic basalt with abundant large olivine pseudomorphs, rare fresh olivine, and clinopyroxene.

Sideromelane forms during submarine eruptions of basaltic magma when magma is quenched in seawater, and therefore is relatively abundant in volcaniclastic sediments formed during the submarine shield-building stage of ocean island volcanoes (Fisher and Schmincke, 1984). In contrast, lithic clasts formed during subaerial basaltic eruptions are generally of two types: (1) tachylitic basalt, which forms as subaerially erupted basaltic lava flows into the sea and is quenched, and (2) crystalline basalt fragments, especially red oxidized clasts. The proportions of sideromelane relative to tachylite and crystalline lithic clasts in volcaniclastic sediments can be used as an indicator of the relative contributions of submarine and subaerially erupted basalts (Schmincke and von Rad, 1979). The lowermost (middle Miocene) part of the sedimentary sequence at Site 953 consists of a section that is dominated by sideromelane, overlain by a transition region in which the proportion of sideromelane decreases rapidly to low values (Fig.2). This sequence probably corresponds to the transition from the shallow submarine to emergent shield stages of Gran Canaria.

Bulk chemical analyses of the volcaniclastic sediments indicate low SiO_2 contents, high MgO (≤17 wt%), and high concentrations of compatible trace elements (Ni mostly 400–860 ppm, Cr 161–1100 ppm, V 150–780 ppm; Shipboard Scientific Party, 1995a). In particular, the very high Ni contents and the abundance of large olivine pseudomorphs indicate that picritic magmas were dominant during the submarine and shallow emergent shield phases that are represented by this unit. Picritic basalts have also been found in subaerial exposures of Miocene age on Gran Canaria (Hoernle and Schmincke, 1993). Within the hyaloclastite sequence, the poor sorting, slight reverse grading at the base of each depositional unit, and the matrix-supported nature of many of the very thick-bedded deposits suggest that emplacement occurred by multiple debris flows. However, the vesicular nature of the altered glass shards suggests that they were originally formed during shallow submarine eruptions.

Site 956

The oldest volcaniclastic sediments recovered from Site 956, located to the southwest of Gran Canaria (Fig. 1), consist of hyaloclas-

tite tuff, lapillistone, and breccia of middle Miocene age (Shipboard Scientific Party, 1995b). These sediments are petrographically similar to volcaniclastic sediments of similar age recovered at Site 953, overlying the older picritic hyaloclastites described above (Fig. 2). The volcaniclastic sediments from the lowermost sequence at Site 956 are quite variable in mineralogy and texture, and consist dominantly of moderately evolved basaltic, rather than picritic, material. Furthermore, the sediments at Site 956 contain a greater abundance of subaerially-erupted basalt clasts (Fig. 2), especially the breccias, which contain abundant clasts of vesicular basalt and red oxidized scoriaceous fragments. These units also contain a moderate amount of altered vesicular glass shards, indicating that hydroclastic eruptions were occurring on the southwest side of Gran Canaria during this time and that the products of both submarine and subaerial volcanism were mixed together before deposition of the coarse clastic units. The subaerial equivalents of the Miocene hyaloclastites at Site 953 (picritic) and Site 956 (differentiated basalt) range in composition from tholeiitic to mildly alkalic (Hoernle and Schmincke, 1993; Gurenko et al., 1996).

SAMPLE PREPARATION

Pyroxene separates were prepared by crushing samples of hyaloclastite tuff and lapillistone, sieving to the 1000- to 355-µm size fraction, and handpicking the crystals. Each separate was then placed in a shallow dish filled with refractive index oil (n = 1.657) and viewed under a binocular microscope. This allows individual inclusion-bearing crystals to be carefully examined to avoid samples in which small cracks are observed radiating out from the inclusion into the surrounding host mineral. This is an important step in sample characterization because it avoids inclusions that may have lost dissolved volatiles from syn- or posteruptive cracking of the host mineral. Many of the inclusions found in pyroxenes from the hyaloclastite samples were pervasively altered to clay, probably as a result of seawater or pore water infiltrating along cracks in the pyroxene host. Inclusions that remained glassy in these >14-Ma marine sediments must have been free of any cracks. Such inclusions should not have been affected either by syn-eruptive degassing or postemplacement hydration. However, the analytical data presented below reveal that several inclusions did undergo low temperature (secondary) hydration.

Pyroxene crystals containing glass inclusions were mounted on a microscope slide using acetone-soluble cement. Doubly polished wafers with two parallel sides were prepared from the inclusion-bearing crystals so that both sides of the wafer intersected the inclusion(s). Individual crystals were oriented before grinding so that the maximum number of inclusions would be intersected by the polished surfaces. Some crystals with very small inclusions were prepared so that only one side of the inclusion was intersected by the polished surface. To ensure uniform sample thickness during grinding, the samples were periodically viewed under a petrographic microscope to observe the distribution of interference colors. Photomicrographs of the inclusions analyzed in this study are shown in Figure 3.

The thickness of each inclusion was measured by mounting the edge of the doubly polished pyroxene wafer to a needle using epoxy and immersing the wafer into a cylindrical glass well filled with refractive index liquid (n = 1.657). This allows the crystal to be rotated and viewed parallel to the flat dimension under a microscope with a calibrated eyepiece, thereby allowing a direct measurement of the thickness. For inclusions with both sides intersected by the surfaces of the pyroxene wafer, these measurements have an accuracy of ±1 to ±3 µm, depending on how close the inclusion is to the edge of the wafer; inclusions located close to the center of a pyroxene wafer are generally more poorly resolved. The results of this measurement technique agree with measurements made using a digital micrometer (Skirius, 1990). Thickness measurements for small inclusions that are intersected only by one side of the pyroxene wafer are generally less accurate.

INFRARED SPECTROSCOPY

Transmission infrared (IR) spectra of the glass inclusions were obtained using a Nicolet Magna 550 Fourier transform infrared spectrometer equipped with a Spectratech IR-Plan analytical microscope at the U.S. Geological Survey, Menlo Park, California. This instrument has upper and lower (redundant) apertures that can be used to direct the beam path through the doubly polished glass inclusions and avoid the surrounding pyroxene host (Fig. 4). Inclusions were analyzed using either fixed diameter circular apertures that yield a 100-µm-diameter region or adjustable knife-edged apertures for smaller inclusions. A KBr beamsplitter and liquid nitrogen-cooled $HgCdTe_2$ (MCT) detector were used for all spectra.

Band assignments for dissolved water and carbonate in basaltic glass were made as described in Dixon et al. (1995). Quantitative determination of the total amounts of dissolved H_2O (determined from the OH^- band) and CO_2 (determined from the carbonate bands) were made using Beer's law:

$$c = \frac{(mol.\ wt.)(abs)}{\rho \cdot d \cdot \varepsilon}$$

where c is the concentration, in weight fraction, of the absorbing species, *mol. wt.* is the molecular weight (18.02 for OH^- and 44.00 for CO_3^{2-}), *abs* is the absorbance intensity of the band of interest, ρ is the room temperature density of the glass, d is thickness (path length), and ε is the molar absorption coefficient. A glass density of 2800 kg/m^3 was assumed for all inclusions.

Total dissolved water was measured using the intensity of the broad, asymmetric band centered at 3530 cm^{-1} (Fig. 5A), which corresponds to the fundamental OH-stretching vibration (Nakamoto, 1978). Absorbance intensity of the 3530 cm^{-1} band for each sample was measured as the peak height from the plotted spectrum using a graphical background subtraction procedure in which the background was drawn as a smooth curve. Total dissolved water contents (Table 1) were calculated using a molar absorption coefficient of 63 ± 3 L/mol-cm (Dobson et al., unpubl. data, as cited in Dixon et al., 1995). To examine the speciation of water in these glasses as a means of screening for low temperature hydration, concentrations of dissolved molecular H_2O were determined by measuring the intensity of the 1630 cm^{-1} absorption band, which corresponds to the fundamental bending mode of dissolved water molecules (Nakamoto, 1978). Unlike the molar absorptivity for the 3530 cm^{-1} band, which is relatively independent of composition for basaltic glasses, Dixon et al. (1995) have shown that the molar absorptivity for molecular water is compositionally dependent. Using the method described in Dixon et al. (1995), together with the average composition of the glass inclusions (P. Wallace, unpubl. data) that have detectable molecular water, the molar absorptivity of the 1630 cm^{-1} band is 21 ± 4 L/mol-cm.

Dissolved carbonate was measured from the absorbances of the bands at 1515 and 1430 cm^{-1} (Fig. 5B), which correspond to antisymmetric stretching of distorted carbonate groups (Brey and Green, 1975; Fine and Stolper, 1986; Dixon et al., 1995). Illustrated in Figure 5B is the spectrum of a typical basaltic glass inclusion showing the carbonate bands. The shape of the background in the region of the carbonate doublet is complex (Dixon et al., 1995). Absorbance intensities for the 1515 and 1430 cm^{-1} bands were measured after subtraction of a reference spectrum for a decarbonated basaltic glass to achieve a relatively flat background (Dixon et al., 1995). The molar absorptivity for carbon dissolved as carbonate in basaltic glasses is compositionally dependent (Dixon and Pan, 1995). Dissolved carbonate contents (reported in Table 1 and hereafter as the equivalent amount of CO_2 in parts per million) were determined using a molar

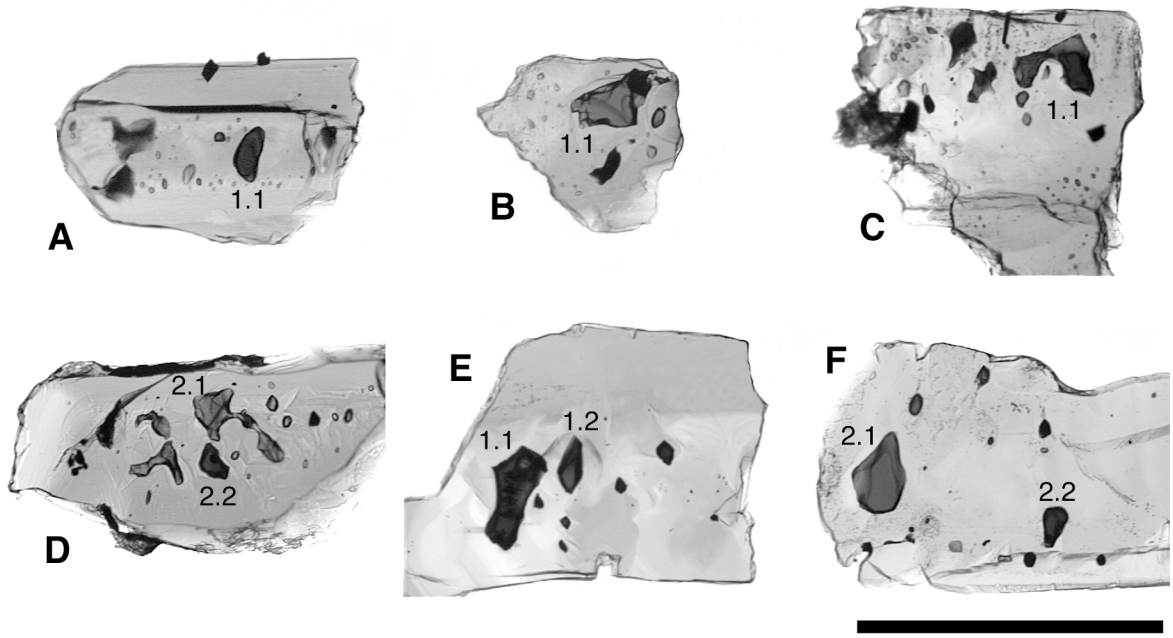

Figure 3. Photomicrographs of inclusion-bearing pyroxene crystals after sectioning for IR spectroscopy. **A.** Sample 157-953C-97R-4, 27–34 cm. **B.** Sample 157-953C-100R-5, 26–30 cm. **C**, **D.** Sample 157-953C-102R-2, 46–51 cm. **E**, **F.** Sample 157-956B-50R-3, 44–48 cm. Each analyzed glass inclusion is denoted by a number (e.g., 1.1) corresponding to the analyses in Table 1. A 1-mm scale bar is shown at the lower right.

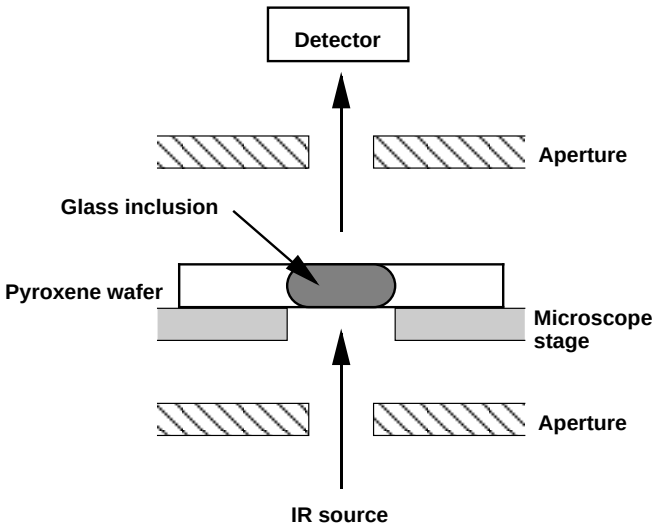

Figure 4. Schematic diagram showing the geometry used to obtain IR transmission spectra using a Nicolet Magna 550 FT-IR, equipped with a Spectra-tech IR-plan analytical microscope. Further description of the apertures used is given in the text.

absorption coefficient of 340 L/mol-cm, calculated from the average composition of the glass inclusions and the linear equation reported by Dixon and Pan (1995).

For small glass inclusions in which only one side of the inclusion is intersected by the polished surface of the pyroxene wafer, the IR spectrum contains contributions from both basaltic glass and pyroxene. This causes an additional complication in measuring absorbance intensities for the carbonate doublet because of the presence of an absorbance band in pyroxene centered at ~1520 cm^{-1} (Fig. 6). To subtract the contribution from pyroxene from such spectra, an IR spectrum was also taken for each of the pyroxene crystals. The factor by which the pyroxene spectrum was scaled for each subtraction was determined empirically so that the carbonate bands in the pyroxene-subtracted glass spectrum had equal absorbance intensities (Fig. 6). Subtraction of the decarbonated basaltic glass reference spectrum was performed after subtraction of the pyroxene spectrum.

RESULTS

The dissolved H_2O and CO_2 concentrations of glass inclusions from Holes 953C and 956B are listed in Table 1. Inclusions from Hole 953C (picrites) generally have very low dissolved water contents (0.08–0.15 wt%), with one sample (157-953C-100R-5, 26–30 cm) having a higher water content of 0.45 wt%. In contrast, inclusions from Hole 956B (differentiated basalts) have higher total dissolved H_2O contents ranging from 0.57 to 1.38 wt%.

Concentrations of dissolved molecular H_2O in the glass inclusions are quite variable (Table 1). If the inclusions have not been affected by low temperature hydration, then the concentration of dissolved molecular water should be close to the high-temperature water speciation curve for basaltic glasses (Dixon et al., 1995). The plot shown in Figure 7 demonstrates that for eight of the 11 inclusions, the concentrations of molecular water are within error (±20%) of the high-temperature speciation curve. The remaining three inclusions clearly have excess molecular water over what would be expected for high-temperature equilibrium. For two of these, subtraction of the excess molecular water yields total dissolved water concentrations of 0.08 and 0.20 wt%, suggesting that before hydration, these inclusions had total water concentrations similar to many of the other inclusions. These corrected water contents will be used for subsequent discussion and calculations (Table 1). Secondary hydration of inclusion 1.2 from Sample 157-956B-50R-3, 44–48 cm, has been much more intense, as the total dissolved water and dissolved molecular water concentrations are comparable (Table 1). This inclusion probably had low initial total H_2O, but the large uncertainty in dissolved molecular water

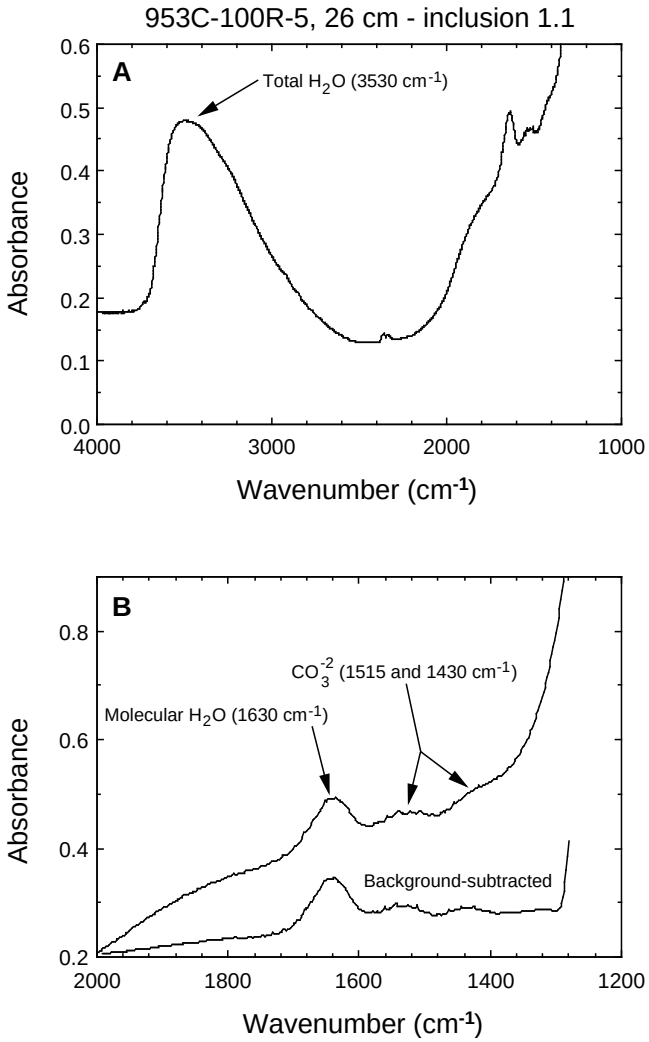

Figure 5. **A.** IR spectrum of a basaltic glass inclusion from the hyaloclastites in Hole 953C showing the fundamental OH-stretching vibration (3530 cm^{-1}) used for quantitative determination of dissolved water concentrations in the glass. **B.** Enlargement of the 1200–2000 cm^{-1} region in A showing positions of the carbonate doublet used for determination of the dissolved carbonate concentration and the band at 1630 cm^{-1} that is caused by molecular water in the glass. Also shown is the spectrum after background subtraction using a decarbonated basaltic glass, as described in the text.

makes it difficult to estimate the water concentration before hydration (Fig. 7).

Dissolved carbonate concentrations in the glass inclusions are, with one exception, between 100 and 350 ppm (Table 1). Inclusions from Hole 956B generally have lower CO_2 contents that those from Hole 953C. One inclusion from Hole 953C (interval 157-953C-102R-2, 46–51 cm, inclusion 2.2) contains 1426 ppm CO_2, much higher than any other sample, including another inclusion (2.1) in the same pyroxene crystal.

The dissolved H_2O and CO_2 concentrations of the inclusions are shown in Figure 8, together with H_2O-CO_2 vapor saturation curves for basaltic melts at pressures of 100 to 2000 bars and a temperature of 1200°C. If the trapped melts that were quenched to form the glass inclusions were vapor-saturated during crystallization of pyroxene and entrapment of inclusions, then the dissolved H_2O and CO_2 contents can be used to calculate the pressure at which crystallization occurred (Table 1). If the melts were not vapor-saturated, then the H_2O and CO_2 data provide a minimum pressure of crystallization. However, because of the very low solubility of CO_2 in silicate melts, basaltic melts will generally be vapor-saturated at crustal pressures, as evidenced by the occurrence of dense liquid CO_2 inclusions in olivine from basaltic magmas worldwide (Roedder, 1965). Despite the wide range in dissolved water concentrations, the pressures indicated by the H_2O and CO_2 data are generally similar, with an average value of 500 ± 100 (1σ) bars (excluding the high CO_2 inclusion).

Shown in Figure 9 is a comparison of the H_2O and CO_2 data for glass inclusions from the shield-building stage of Gran Canaria with data determined by IR spectroscopy on a variety of basaltic glasses. These samples include tholeiitic glass inclusions in olivine phenocrysts from the 1959 Kilauea Iki picritic eruption (Anderson and Brown, 1993), submarine-erupted tholeiitic glasses from Kilauea's east rift zone (ERZ; Dixon et al., 1991), submarine-erupted alkali basalt through nephelinite composition glasses from the North Arch volcanic field, located on the seafloor north of Hawaii (Dixon et al., 1997), and submarine-erupted tholeiitic glasses from the Juan de Fuca Ridge and nearby seamounts (Dixon et al., 1988). Most of the glass inclusions from Sites 953 and 956 have very low total dissolved water. These water concentrations are comparable to the lowest values that have been recorded for the Juan de Fuca Ridge glasses (Dixon et al., 1988) and for mid-ocean-ridge basalt (MORB) tholeiitic glasses from other spreading ridges (Muenow et al., 1990). The low-H_2O inclusions from Gran Canaria have significantly lower total dissolved water (average 0.12 ± 0.04 wt%) than the glass inclusions from Kilauea Iki (average 0.54 ± 0.21 wt%), the submarine-erupted glasses from Kilauea ERZ (average 0.51 ± 0.17 wt%), or the silica-undersaturated glasses from the North Arch volcanic field (average 0.98 ± 0.19 wt%). In contrast, two inclusions from the evolved basaltic hyaloclastites (Site 956) have significantly higher total dissolved H_2O than tholeiitic glasses and glass inclusions from Kilauea volcano and the Juan de Fuca Ridge and are comparable to the highest water concentrations found in the Hawaiian North Arch glasses (Fig. 9).

When comparing the CO_2 contents of glasses from these data sets, it is important to note that because of the strong pressure dependence of CO_2 solubility in basaltic melts, the measured CO_2 contents in submarine-erupted basaltic glasses commonly reflect the pressure at the depth of eruption and quenching (e.g., North Arch and Kilauea ERZ), or for kinetic reasons are intermediate between the inferred pressure of pre-eruptive storage and that of the depth of quench (e.g., Juan de Fuca Ridge; see Dixon and Stolper [1995], and references therein, for a complete discussion). In contrast, the CO_2 contents of glass inclusions in phenocryst minerals reflect the pressure at which crystallization occurred. Nevertheless, all the inclusions from the samples from Sites 953 and 956, with the exception of the single high-CO_2 inclusion, have CO_2 contents close to the average values for the glasses and glass inclusions from tholeiitic basalts. The Gran Canaria samples, however, have much lower CO_2 contents than the North Arch glasses, which were erupted and quenched in relatively deep water (~4000 m; Clague et al., 1990). The single high-CO_2 inclusion from Sample 157-953C-102R-2, 46–51 cm, must have formed at a minimum pressure of ~2800 bars.

DISCUSSION

Comparison of the data from Sites 953 and 956 with similar data from Kilauea volcano and with the results of experimental studies on volatile solubilities in basaltic melts reveals several interesting features regarding the physical processes of magma ascent, storage, crystallization, and eruption during the Miocene shield-building phase of Gran Canaria. These interpretations should be regarded as preliminary, given the limited number of inclusions that have been analyzed. Additional analyses are needed to assess whether the inclu-

Table 1. Analyses of glass inclusions in clinopyroxene phenocrysts from Leg 157 hyaloclastites.

Sample	Incl.#	n	Total H_2O abs.	Mol. H_2O abs.	CO_3^{2-} abs.	Thickness (microns)	Total H_2O (wt%)	Mol. H_2O (wt%)	Corr. H_2O (wt%)	CO_2 (ppm)	P_{sat} (bars)
157-953C-											
97R-4, 27–34	1.1	2	0.076	—	0.036	75	0.10	—	—	221	480
100R-5, 26–30	1.1	3	0.327	0.091	0.023	75	0.45	0.37	0.08	142	310
102R-2, 46–51	1.1	3	0.161	—	0.080	108	0.15	—	—	344	740
	2.1	2	0.059	—	0.031	70	0.09	—	—	207	450
	2.2	1	0.095	—	0.216[b]	70	0.14	—	—	1426	2800
103R-2, 72–77	1.1	2	0.037	—	0.027	50	0.08	—	—	247	530
	1.2	1	0.058	—	0.037	70	0.08	—	—	243	520
157-956B-											
50R-3, 44–48	1.1	2	0.375[a]	0.081	0.021	67	0.57	0.37	0.20	141	310
	1.2	1	0.662	0.220	0.031	60	1.13	1.12	—	239	-
	2.1	3	0.673	0.062	0.015	50	1.38	0.38	—	140	500
	2.2	1	0.600	0.040	0.012	50	1.23	0.25	—	106	390

Notes: Inclusion numbers (Incl.#) are in the format x.y, where x is the crystal and y is the inclusion (e.g., 2.1 and 2.2 are different inclusions in the same crystal). Absorbance intensities for total water (3530 cm^{-1}), molecular H_2O (1630 cm^{-1}), and carbonate (1515 and 1430 cm^{-1}) were determined by IR spectroscopy, as described in the text. Multiple spectra were taken of most inclusions; the reported absorbances and calculated H_2O and CO_2 concentrations for inclusions with n = 2 or 3 represent average values. Inclusion thicknesses (d), in µm, were measured using a microscope with a calibrated eyepiece, as described in the text. H_2O and CO_2 contents were calculated using absorption coefficients from Dobson et al. (unpubl. data, cited in Dixon et al., 1995), Dixon and Pan (1995), and Dixon et al. (1995); see text for further discussion. A room-temperature glass density of 2800 kg/m^3 was assumed for all inclusions. Based on multiple analyses of individual inclusions, the precision of the spectroscopic measurement for the 3530 cm^{-1} band is 2%–10% (relative), except for the very low water content inclusions, for which it is ±0.01 to ±0.02 wt% (absolute). The average precision for the 1515 and 1430 cm^{-1} bands is ~10% (relative). Accuracies are limited by uncertainties in molar absorption coefficients and in the background correction procedures, and have been estimated to be ~10% for the measurement of total dissolved H_2O contents and ~15% for carbonate (Dixon et al., 1988, 1995). For two of the inclusions that have been affected by low-temperature hydration, a corrected value for the total H_2O concentration before hydration (Corr. H_2O) has been estimated by subtracting the excess molecular H_2O. No corrected value is given for inclusion 157-956B-50R-3, 44–48 cm (1.2), because it has undergone more substantial hydration. Pressures (P_{sat}) at which basaltic melt would be saturated with a vapor phase containing H_2O and CO_2 were calculated using experimental solubility data (Dixon et al., 1995).

[a] The H_2O content in this inclusion was inhomogeneous. Spectra taken in one region of the inclusion yielded an average value of 0.57 wt%, whereas those from another region near a large vapor bubble yielded 0.96 wt%. Comparison of measured concentrations of molecular H_2O with those expected for high temperature speciation of water in basaltic melts indicates that these differences are because of low-temperature hydration of the glass and that the extent of hydration is most intense near the vapor bubble. Based on the equilibrium speciation curve, the total dissolved H_2O in this inclusion before secondary hydration is estimated to be ~0.2 wt%.

[b] This nclusion contained a vapor bubble that was close to the glassy region analyzed by IR spectroscopy. Some of the bubble may have been in the beam path during acquisition of the spectrum. However, the bubble should contain molecular CO_2 vapor that would not contribute to the absorbance intensity of the carbonate bands, unless a carbonate mineral has formed on the bubble wall due to reaction of the glass with vapor in the bubble. There is no petrographic evidence of any such mineralization on the vapor bubble wall.

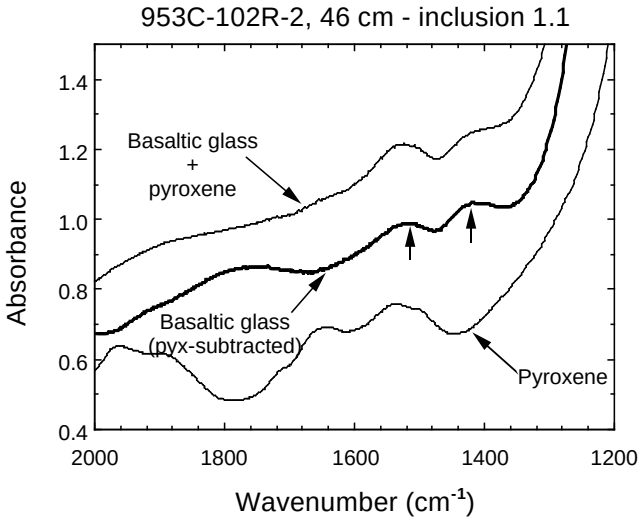

Figure 6. Example of spectra used in the subtraction procedure for inclusions that were intersected only on one side of the pyroxene (pyx) wafer. A description of this procedure is given in the text. The two short vertical arrows indicate the carbonate doublet at 1515 and 1430 cm^{-1}; these bands have equal intensities in the pyroxene-subtracted glass spectrum.

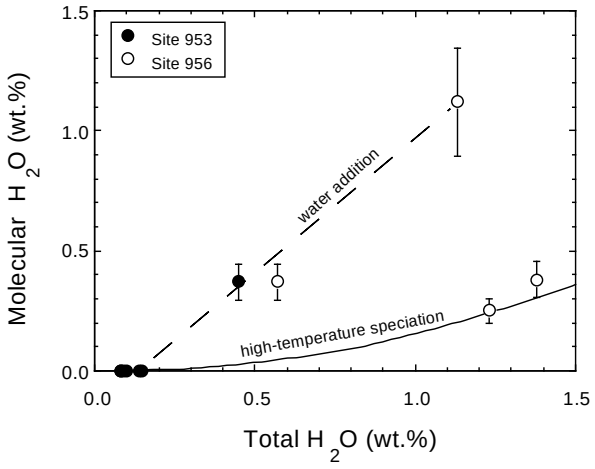

Figure 7. Total dissolved H_2O and dissolved molecular H_2O in glass inclusions. Data are shown for glass inclusions from the Miocene picritic sequence from Site 953 and for the moderately evolved basaltic sequence from Site 956. Shown for comparison is the experimentally determined high-temperature speciation model for water in tholeiitic glass (Dixon et al., 1995). Three of the glass inclusions show an excess of molecular water that probably is the result of low-temperature hydration.

sion data in Table 1 are truly representative of middle Miocene basaltic volcanism on Gran Canaria.

Dynamics of Magma Ascent, Storage, and Crystallization

One of the most noteworthy features of Sites 953 and 956 glass inclusion data is that despite differences in bulk composition (picrite vs. evolved basalt) and inferred eruptive locations (north vs. south sides of Gran Canaria) of samples from the two sites, calculated vapor saturation pressures indicate that pyroxene crystallization occurred at similar pressures (500 ± 100 bars). Such low pressures of crystallization (equivalent to ~1 to 3 km depth beneath the top of the edifice) are surprising for the picritic magmas from which Site 953 hyaloclastites were formed. Phenocrysts in little-differentiated, man-

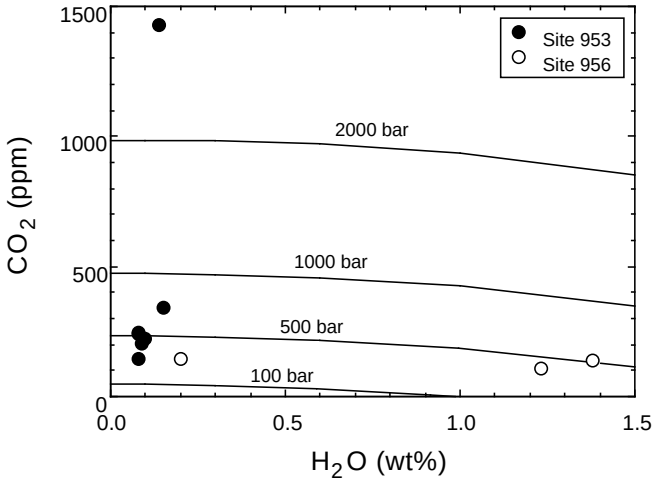

Figure 8. Total dissolved H_2O and CO_2 concentrations in glass inclusions. All samples were analyzed using the methods described in Table 1. For two of the samples that were affected by low-temperature hydration, the corrected value for total dissolved H_2O is used (see text and Table 1 for discussion). Diagonal lines = H_2O and CO_2 contents of basaltic melt saturated with H_2O-CO_2 vapor at pressures from 100 to 2000 bars and a temperature of 1200°C. The lines have negative slopes because the amounts of dissolved H_2O and CO_2 are proportional to their fugacities (f_{H_2O} and f_{CO_2}, respectively; Dixon et al., 1995), and the sum of the partial pressures of these components (P_{H_2O} and P_{CO_2}) must equal the total pressure in a vapor-saturated melt (f_i is related to P_i by the fugacity coefficient). Thus, at constant total pressure, an increase in f_{H_2O} (and hence dissolved H_2O) must result in a decrease in f_{CO_2} and dissolved CO_2 (Dixon et al., 1995).

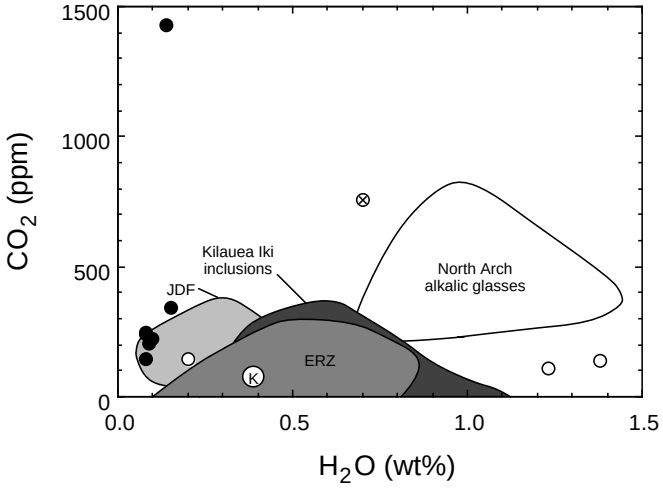

Figure 9. Comparison of the dissolved H_2O and CO_2 concentrations of glass inclusions from Sites 953 (solid circles) and 956 (open circles) with data determined by IR spectroscopy for submarine-erupted basaltic glasses and basaltic glass inclusions from subaerial eruptions. Fields are shown for tholeiitic glass inclusions in olivine phenocrysts from the 1959 Kilauea Iki picritic eruption (Anderson and Brown, 1993), submarine-erupted tholeiitic glasses from Kilauea's ERZ (Dixon et al., 1991), submarine-erupted alkali basalt through nephelinite composition glasses from the North Arch volcanic field located on the seafloor north of Hawaii (Dixon et al., 1997), and submarine-erupted tholeiitic glasses from the Juan de Fuca Ridge and nearby seamounts (JDF; Dixon et al., 1988). The circle labeled "K" indicates the average H_2O and CO_2 contents of high-Mg submarine glasses from the ERZ (Clague et al., 1991). The small circle with an "x" is a glass inclusion from Kilauea Iki that lies outside the range of the other data in the shaded field.

tle-derived magmas are commonly believed to have crystallized at much greater pressures, reflecting lower crustal to upper mantle depths (Roedder, 1965). Indeed, crystallization pressures for Miocene picrites on Gran Canaria were estimated to be ~5 kbar by Gurenko et al. (1996), based on comparison with experimental phase equilibria involving cotectic crystallization of olivine and clinopyroxene in tholeiitic magma (Eggins, 1992). The entrapment pressure of ~2800 bars for the single high-CO_2 glass inclusion from Site 953 does indicate that some crystallization of clinopyroxene (and presumably olivine) occurred at relatively high pressures.

In contrast to the estimate based on phase equilibria, Gurenko et al. (1996) report that CO_2-rich fluid inclusions in olivines from subaerial Miocene picrites on Gran Canaria indicate pressures of ~1 kbar. This evidence for crystallization of olivine at relatively low pressures is more consistent with the results presented here for the dominantly low-pressure crystallization of clinopyroxene. One potential explanation for the apparent discrepancy between pressure estimates based on phase equilibrium and those based on glass and fluid inclusion data could be preferential survival of low-pressure inclusions during eruptive decompression (Tait, 1992). However, this is unlikely to be an important factor for the Gran Canaria picrites, as they likely crystallized over a temperature interval of ~300°C (Gurenko et al., 1996). Inclusions that experience a decrease in temperature after entrapment are unlikely to become overpressured as in the isothermal case considered by Tait (1992).

Low-pressure crystallization of olivine phenocrysts in the 1959 Kilauea Iki picrite has recently been demonstrated by Anderson and Brown (1993). They noted that pressures deduced from glass inclusions correspond to those estimated from geodetic and seismic data for the upper part of Kilauea's summit magma reservoir (Ryan, 1987), and they suggested that most crystallization occurred fairly rapidly when an ascending new batch of picritic magma intruded a shallow, stored body of magma beneath Kilauea's summit region. Anderson and Brown (1993) proposed that eruption of picritic magmas occurs rarely at Kilauea, because new batches of mantle-derived melt typically ascend within Kilauea's primary conduit (Ryan, 1988) and intrude into more differentiated magmas at depths where the picritic magmas are more dense than the differentiated magma. Thus, each new batch of magma ponds beneath the stored magma and provides heat and mass to sustain the long-lived summit reservoir. In contrast, Anderson and Brown (1993) suggested that during the period from 1924 to 1959, the summit reservoir was relatively empty, such that the new 1959 picritic magma ascended through an unusual route and first encountered stored magma at an unusually shallow level. Anderson and Brown (1993) and Anderson (1995) demonstrated that a picritic magma with a bulk CO_2 content of 0.3 wt% would be positively buoyant relative to stored, degassed tholeiite at pressures <~2 kbar because of the low density of exsolved CO_2-rich gas in the picrite.

This explanation for the dynamics of Kilauea's magmatic system may be relevant to the Miocene shield-building stage of Gran Canaria. Whether ascending batches of picritic magma at Gran Canaria were positively buoyant with respect to stored magma depends both on the bulk CO_2 content of the picritic magma and the depth at which it intruded the stored magma (Fig. 10). Evidence for stored, differentiated magma residing at shallow depths comes from the inclusions in the moderately evolved basaltic hyaloclastites at Site 956. Based on geodetic studies and a profile of in situ density vs. depth derived from a gravity inversion study of the summit and flanks of Kilauea and Mauna Loa, Ryan (1987) argued that shallow magma storage at these volcanoes occurs in a region of neutral buoyancy at 2- to 4-km depth. If shallow magma storage occurred over a similar range of depths (equivalent to pressures of ≤1 kbar) during the early Miocene

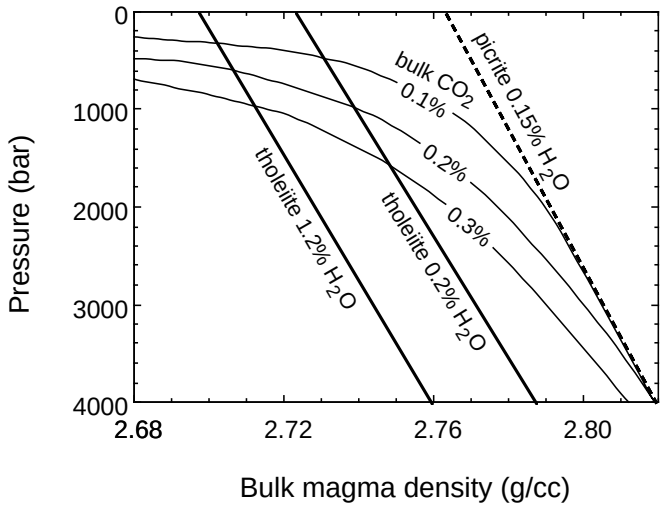

Figure 10. Relationship between pressure, bulk magma density, and bulk (dissolved + exsolved) H_2O and CO_2 contents for picritic and differentiated tholeiitic magmas from the Miocene shield-building stage of Gran Canaria. Densities are shown for CO_2-free tholeiitic melt with 0.2 and 1.2 wt% dissolved H_2O (thick solid lines), CO_2-free picritic melt with 0.15 wt% H_2O (thick dashed line), and for picritic melts with 0.15 wt% H_2O and bulk CO_2 contents of 0.1 to 0.3 wt% (thin solid curves). Major element compositions used in the density calculations are taken from Hoernle and Schmincke (1993). If picritic magmas with ≥0.3 wt% bulk CO_2 intrude shallow stored magma at pressures of 1000–1500 bars, the picritic magma will be positively buoyant and should rise through the differentiated magma, resulting in mixing, cooling, and crystallization (Anderson, 1993). Thus, a gas and crystal-rich cap may form at the top of the stored magma body and be preferentially erupted.

of Gran Canaria, then picritic magmas must have had bulk $CO_2 \geq 0.3$ wt% in order to be positively buoyant relative to the stored magma (Fig. 10).

Water Depths of Submarine Eruptions

If ascent, submarine eruption, and quenching occur rapidly enough so that exsolving vapor is not separated from the magma, then the results of degassing calculations (MacPherson, 1984; Gerlach, 1986; Dixon and Stolper, 1995) using pre-eruptive H_2O and CO_2 contents can be compared with observed vesicularities to constrain the original depth of eruption. This is important because the petrographic and sedimentologic features of the hyaloclastites indicate that emplacement occurred by multiple debris flows that transported vesicular basaltic glass shards originally formed by shallow submarine eruptions. In order to demonstrate that vesicularities calculated with magma degassing models can be used to predict submarine eruption depths, an example from the Kilauea ERZ is shown in Figure 11A. Vesicle contents of submarine glasses from known eruption depths on the ERZ show good correlation with vesicularities calculated from degassing models in which the pre-eruptive H_2O and CO_2 contents are constrained by analyses of the glasses (Fig. 11A). This good correlation suggests that measured vesicularities of basaltic glass shards from the Gran Canaria hyaloclastites can be used to estimate the original depths of eruption and quenching. It should be noted that if the basaltic glass shards were unaltered, as is found in young submarine eruptions, then dissolved H_2O and CO_2 contents of the quenched glass could be measured directly and used as an indicator of the eruption and quenching depth (e.g., Dixon et al., 1991, 1997). However, the glass shards in the hyaloclastites are pervasively altered so that no evidence remains of their original dissolved H_2O and CO_2 contents.

Shown in Figure 11B are two degassing curves, one for a basaltic melt with low dissolved H_2O (0.15 wt%) and the other for a basaltic melt with much higher dissolved H_2O (1.3 wt%). The degassing curves show the calculated vesicularity of each melt as a function of the water depth (pressure) of eruption and quenching. For basaltic magmas with low dissolved H_2O, like those found in the Site 953 inclusions, small amounts of vesicles will be present at pressures >50 bars (eruption in >500 m water depth). Only at very low pressures (<50 bars or <500 m water depth) will such magmas begin to exsolve appreciable amounts of vapor (Fig. 11B). Thus, the presence of vesicularities >~5 vol% would suggest that such magmas were erupted and quenched at very shallow water depths. In contrast, basaltic melts with higher water contents, such as those found in two of the Site 956 glass inclusions (1.2–1.4 wt%), would begin to exsolve significant amounts of vapor at much greater water depths (Fig. 11B). For example, basaltic melts with pre-eruptive dissolved H_2O contents similar to those of some Site 956 inclusions would have vesicularities of ~35 vol% if they were erupted and quenched at 1000 m water depth.

For comparison with these calculated degassing and vesicularity trends, I have measured the vesicle contents of basaltic glass shards in two of the hyaloclastite samples from which glass inclusions were analyzed. Vesicle contents were measured in thin section for the 10 largest glass shards in each sample by using digital images of individual shards and then measuring the area percent occupied by vesicles. These measured area percentages were then corrected to volume percent vesicles by multiplying the area percent by a factor of 1.18 (Cashman and Marsh, 1988; Mangan et al., 1993).

The average vesicularity of glass shards in hyaloclastite Sample 157-953C-97R-4, 27–34 cm, is 16 vol% ± 11 (1σ), with an overall range of 2 to 31 vol% vesicles (Fig. 11C). Based on the vesicularity vs. depth trends shown in Figures 11B and 11C, these data suggest that submarine eruptions of the Miocene picritic basalts (Site 953) occurred at water depths <~500 m. In contrast, the average vesicularity of glass shards from a Site 956 hyaloclastite sample (157-956B-50R-3, 44–48 cm) is 56 vol% ± 18 (Fig. 11D), much higher than for the Site 953 picritic hyaloclastite. The presence of glass inclusions in Sample 157-956B-50R-3, with both low and high dissolved H_2O (Table 1), makes it more difficult to interpret the vesicle data in terms of submarine eruption depths (Fig. 11D). The wide range of observed glass shard vesicle contents could have resulted from very shallow (≤100 m water depth) submarine eruptions of magma with ~0.2 wt% dissolved H_2O. However, the possibility that much of the glass shard–debris in this sample formed in relatively deep water eruptions (400–1200 m) of more H_2O-rich basaltic magmas (~1.3 wt% H_2O) cannot be ruled out.

The presence of glass shards with few to no vesicles in many samples indicates that some material at both Sites 953 and 956 was erupted in water deeper than the estimates given above. A wide range of eruption depths for basaltic magmas that all crystallized at low pressures (~500 bars) might be an indication that during the shield-building phase of Gran Canaria, rift systems similar to those on Kilauea channeled magmas from shallow reservoirs in the central part of the island out to the submarine parts of the flanks.

Implications for Mantle H_2O Contents

Studies of oceanic island basalts have provided a great deal of information on compositional and isotopic heterogeneities that exist in the Earth's upper mantle. In particular, analyses of volatile contents in submarine glassy lavas from oceanic islands have been used to provide constraints on mantle volatile contents (e.g., Clague et al., 1991; Dixon et al., 1997). The generally low dissolved H_2O in picritic magmas from the Miocene shield stage of Gran Canaria may have significant implications for mantle volatile contents and extents of melting beneath this oceanic island volcano. However, recent studies

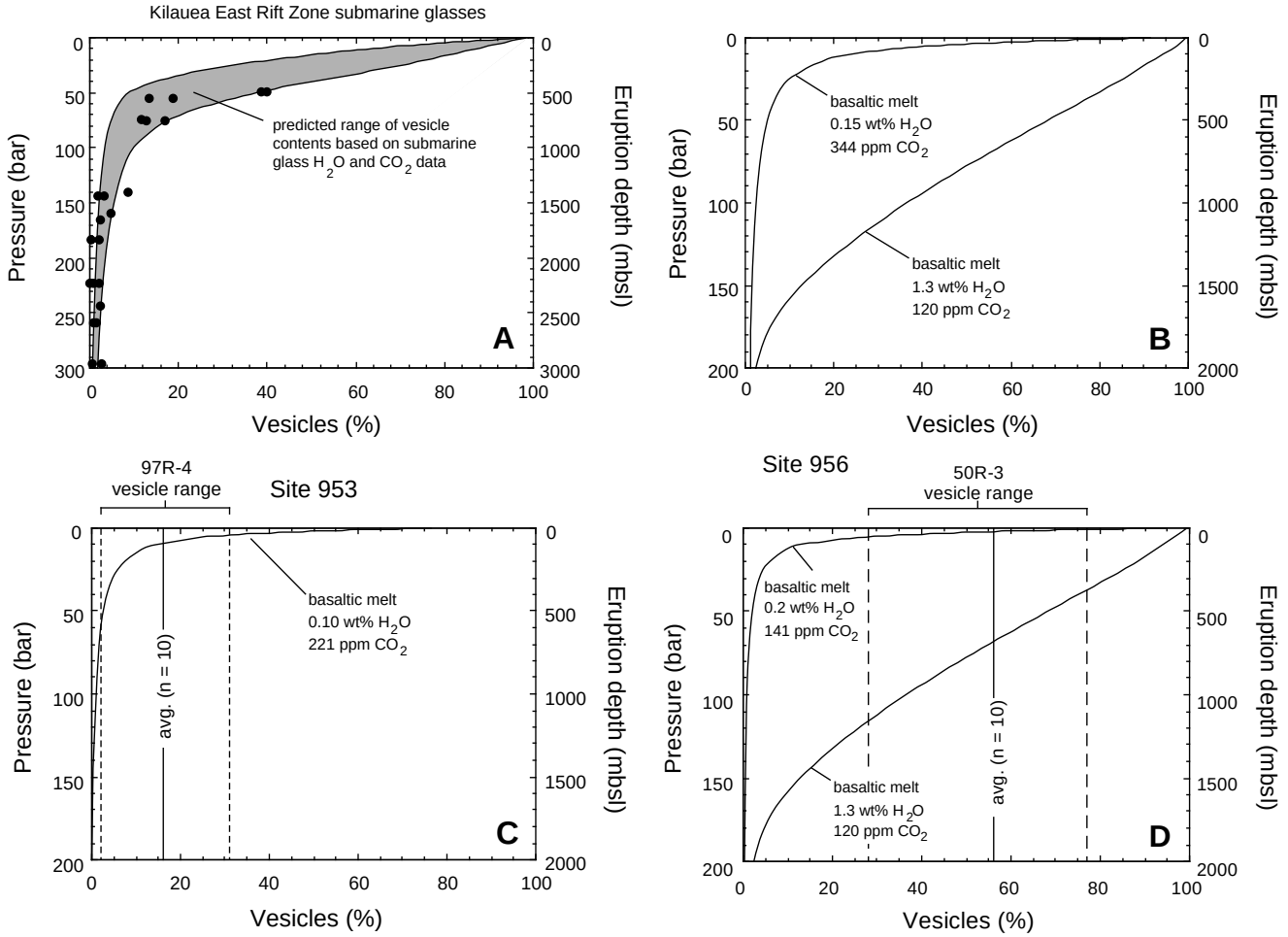

Figure 11. Calculated vesicle contents of basaltic melts as a function of hydrostatic pressure and water depth of eruption. Vesicle contents were calculated using a modified version of a program written by J. Dixon to model degassing of basaltic melts, as described in Dixon and Stolper (1995). All calculations assume closed-system equilibrium exsolution of volatiles from the melt. **A.** Comparison of calculated vs. measured vesicle contents of submarine basaltic glasses of known eruption depths (in meters below sea level [mbsl]) from the ERZ of Kilauea. Vesicle data are from Dixon et al. (1991) and have been converted to vol%, as described in Mangan et al. (1993). The pre-eruptive H_2O and CO_2 concentrations used for the calculated trends are also taken from Dixon et al. (1991) and are based on actual measured values in the same glasses from which the vesicle measurements were made. The values chosen for the calculation are 0.82 wt.% H_2O, 637 ppm CO_2, (sample #1699; Dixon et al., 1991) and 0.44 wt.% H_2O, 297 ppm CO_2 (sample #1714). This range of values encompasses two-thirds of the total range in modeled pre-eruptive H_2O and CO_2 contents of the ERZ glasses (Dixon et al., 1991). **B.** Calculated pressure and eruption depth vs. vesicle content for basaltic melts with dissolved H_2O and CO_2 contents similar to those found in the Miocene glass inclusions from Gran Canaria. **C.** Comparison of calculated vesicle content vs. depth curve for Miocene picritic melts (Site 953) with measured vesicle contents of individual glass shards from hyaloclastite Sample 157-953C-97R-4, 27–34 cm. The average vesicularity of the 10 measured shards is shown by the solid vertical line. The range of vesicle contents is shown by the dashed vertical lines. The glass shard vesicle content data suggest eruption and quenching depths ≤500 bars. **D.** Comparison of calculated vesicle content vs. depth curve for evolved basaltic melts (Site 956) with measured vesicle contents of individual glass shards from hyaloclastite Sample 157-956B-50R-3, 44–48 cm. Estimated eruption and quenching depths for this sample are highly dependent on the assumed initial melt H_2O concentration. See text for discussion.

of Hawaiian volcanism have demonstrated that shallow-level crystallization and degassing in basaltic magma systems can be quite complex (Dixon et al., 1991; Anderson and Brown, 1993; Clague et al., 1995). At Kilauea volcano, mixing of shallow-degassed and undegassed magmas results in a spectrum of dissolved magmatic H_2O concentrations that are lower than those in the original mantle-derived parental magmas (Dixon et al., 1991). Crystallization in such partially degassed magmas can form melt inclusions with low dissolved H_2O contents similar to those found in the Gran Canaria inclusions (Wallace and Anderson, in press). In this context, the single high-pressure inclusion with 0.14 wt% total dissolved H_2O is significant because it is unlikely to have been affected by shallow-level degassing and thus may provide evidence that low water contents were a primary characteristic of some mantle-derived magmas erupted during the shield stage of Gran Canaria.

CONCLUSIONS

Infrared spectroscopic analyses of melt (glass) inclusions in pyroxene crystals from Miocene hyaloclastites recovered from Sites 953 and 956 show a wide range of pre-eruptive dissolved H_2O contents, similar to values reported for both MORB and some Hawaiian (oceanic island) alkalic magmas. Most inclusions have low dissolved H_2O contents (0.08 to ~0.2 wt%), whereas two inclusions from moderately evolved basalt have much higher dissolved H_2O (1.2–1.4

wt%). The speciation of water in these two inclusions is consistent with high-temperature equilibrium for water in basaltic melts, indicating that the high total dissolved H_2O contents are not caused by secondary hydration. All but one inclusion have dissolved carbonate contents between 100 and 350 ppm CO_2. These data form the basis for the following conclusions:

1. The dissolved H_2O and CO_2 contents of nine of the 11 analyzed inclusions demonstrate that pyroxene crystallization occurred at an average pressure of 500 ± 100 bars, equivalent to ~1- to 3-km depth beneath the volcanic edifice of Gran Canaria. Such low pressures of formation are similar to those reported for olivines from the 1959 Kilauea Iki picrite (Anderson and Brown, 1993) and may indicate that during the shield-building phase of Gran Canaria, ascending batches of picritic magma were sufficiently CO_2-rich to be positively buoyant relative to shallow-stored magma.
2. Comparison of degassing models for basaltic melts with measured vesicularities of altered glass shards from the hyaloclastites suggests that much of the glass shard and crystal debris, from which the hyaloclastites were deposited, originally formed in submarine eruptions at water depths <~500 m. Some of the middle Miocene eruptions, however, may have occurred in deeper water (≤1200 m).

ACKNOWLEDGMENTS

I would like to thank J. Lowenstern for assistance with the FT-IR microscope at the U.S. Geological Survey, J. Dixon for providing reference spectra for decarbonated basaltic glasses, A.T. Anderson for many lively discussions concerning the mechanics of Kilauea's magmatic plumbing system, and D. Lorenz and J. Kim for help with sample preparation. Reviews by J. Dixon, J. Lowenstern, and H.-U. Schmincke led to substantial improvements in the final manuscript. Funding for this work was provided by the Joint Oceanographic Institution's U.S. Science Support Program.

REFERENCES

Anderson, A.T., Jr., 1995. CO_2 and the eruptibility of picrite and komatiite. *Lithos,* 34:19–25.

Anderson, A.T., Jr., and Brown, G.G., 1993. CO_2 contents and formation pressures of some Kilauean melt inclusions. *Am. Mineral.,* 78:794–803.

Brey, G.P., and Green, D.H., 1975. The role of CO_2 in the genesis of olivine melilitite. *Contrib. Mineral. Petrol.,* 49:93–103.

Cashman, K.V., and Marsh, B.D., 1988. Crystal size distribution (CSD) in rocks and the kinetics and dynamics of crystallization, II: Makaopuhi lava lake. *Contrib. Mineral. Petrol.,* 99:292–305.

Clague, D.A., Holcomb, R., Sinton, J., Detrick, R., and Torresa, M., 1990. Pliocene and Pleistocene alkalic flood basalts on the seafloor north of the Hawaiian islands. *Earth Planet. Sci. Lett.,* 98:175–191.

Clague, D.A., Moore, J.G., Dixon, J.E., and Friesen, W.B., 1995. Petrology of submarine lavas from Kilauea's Puna Ridge, Hawaii. *J. Petrol.,* 36:299–349.

Clague, D.A., Weber, W.S., and Dixon, J.E., 1991. Picritic glasses from Hawaii. *Nature,* 353:553–556.

Dixon, J.E., Clague, D.A., Poreda, R., and Wallace, P., 1997. Volatiles in alkalic basalts form the North Arch Volcanic Field, Hawaii: extensive degasssing of deep submarine-erupted alkalic series lavas. *J. Petrol.,* 38:911–939.

Dixon, J.E., Clague, D.A., and Stolper, E.M., 1991. Degassing history of water, sulfur, and carbon in submarine lavas from Kilauea volcano, Hawaii. *J. Geol.,* 99:371–394.

Dixon, J.E., and Pan, V., 1995. Determination of molar absorptivity of dissolved carbonate in basanitic glass. *Am. Mineral.,* 80:1339–1342.

Dixon, J.E., and Stolper, E.M., 1995. An experimental study of water and carbon dioxide solubilities in mid-ocean ridge basaltic liquids. Part II: Applications to degassing. *J. Petrol.,* 36:1633–1646.

Dixon, J.E., Stolper, E., and Delaney, J.R., 1988. Infrared spectroscopic measurements of CO_2 and H_2O in Juan de Fuca Ridge basaltic glasses. *Earth Planet. Sci. Lett.,* 90:87–104.

Dixon, J.E., Stolper, E.M., and Holloway, J.R., 1995. An experimental study of water and carbon dioxide solubilities in mid-ocean ridge basaltic liquids. Part I: Calibration and solubility models. *J. Petrol.,* 36:1607–1631.

Eggins, S.M., 1992. Petrogenesis of Hawaiian tholeiites: 1. Phase equilibria constraints. *Contrib. Mineral. Petrol.,* 110:387–397.

Fine, G., and Stolper, E., 1986. Dissolved carbon dioxide in basaltic glasses: concentrations and speciation. *Earth Planet. Sci. Lett.,* 76:263–278.

Fisher, R.V., and Schmincke, H.-U., 1984. *Pyroclastic Rocks*. Berlin:Springer-Verlag.

Gerlach, T.M., 1986. Exsolution of H_2O, CO_2, and S during eruptive episodes at Kilauea Volcano, Hawaii. *J. Geophys. Res.,* 91:12,177–12,185.

Gurenko, A.A., Hansteen, T.H., and Schmincke H.-U., 1996. Evolution of parental magmas of Miocene shield basalts of Gran Canaria (Canary Islands): constraints from crystal, melt and fluid inclusions in minerals. *Contrib. Mineral. Petrol.,* 124:422–435.

Hoernle, K., and Schmincke, H.-U., 1993. The petrology of the tholeiites through melilite nephelinites on Gran Canaria, Canary Islands: crystal fractionation, accumulation, and depth of melting. *J. Petrol.,* 34:573–578.

MacPherson, G.J., 1984. A model for predicting the volumes of vesicles in submarine basalts. *J. Geol.,* 92:73–82.

Mangan, M.T., Cashman, K.V., and Newman, S., 1993. Vesiculation of basaltic magma during eruption. *Geology,* 21:157–160.

Muenow, D.W., Garcia, M.O., Aggrey, K.E., Bednarz, U., and Schmincke, H.-U., 1990. Volatiles in submarine glasses as a discriminant of tectonic origin: application to the Troodos ophiolite. *Nature,* 343:159–161.

Nakamoto, K., 1978. *Infrared and Raman Spectra of Inorganic and Coordination Compounds* (3rd ed.): New York: Wiley.

Roedder, E., 1965. Liquid CO_2 inclusions in olivine-bearing nodules and phenocrysts from basalts. *Am. Mineral.,* 50:1746–1782.

Ryan, M.P., 1987. Neutral buoyancy and the mechanical evolution of magmatic systems. *In* Mysen, B.O. (Ed.), *Magmatic Processes: Physicochemical Principles.* Geochem. Soc.

————, 1988. The mechanics and three-dimensional internal structure of active magmatic systems: Kilauea Volcano, Hawaii. *J. Geophys. Res.,* 93:4213–4248.

Schmincke, H.-U., 1982. Volcanic and chemical evolution of the Canary Islands. *In* von Rad, U., Hinz, K., Sarnthein, M., and Seibold, E. (Eds.), *Geology of the Northwest African Continental Margin:* Berlin (Springer), 273–306.

————, 1994. *Geological Field Guide: Gran Canaria* (6th ed.): Kiel, Germany (Pluto Press).

Schmincke, H.-U., and von Rad, U., 1979. Neogene evolution of Canary Island volcanism inferred from ash layers and volcaniclastic sandstones of DSDP Site 397 (Leg 47A). *In* von Rad, U., Ryan, W.B.F., et al., *Init. Repts. DSDP,* 47 (Pt. 1): Washington (U.S. Govt. Printing Office), 703–725.

Schmincke, H.-U., Weaver, P.P.E., Firth, J.V., et al., 1995. *Proc. ODP, Init. Repts.,* 157: College Station, TX (Ocean Drilling Program).

Shipboard Scientific Party, 1995a. Site 953. *In* Schmincke, H.-U., Weaver, P.P.E., Firth, J.V., et al., *Proc. ODP, Init. Repts.,* 157: College Station, TX (Ocean Drilling Program), 317–394.

————, 1995b. Site 956. *In* Schmincke, H.-U., Weaver, P.P.E., Firth, J.V., et al., *Proc. ODP, Init. Repts.,* 157: College Station, TX (Ocean Drilling Program), 497–557.

Skirius, C.M., 1990. Pre-eruptive H_2O and CO_2 content of plinian and ash-flow Bishop Tuff magma [Ph.D. dissert.]. Univ. of Chicago.

Tait, S., 1992. Selective preservation of melt inclusions in igneous phenocrysts. *Am. Mineral.,* 77:146–155.

Wallace, P., and Anderson, A.T., Jr., in press. Effects of eruption and lava drainback on the H_2O contents of basaltic magmas at Kilauea. *Bull. Volcanol.*

Date of initial receipt: 8 July 1996
Date of acceptance: 6 January 1997
Ms 157SR-146

Prior Chapter Contents Next Chapter